# Supporting Information

## Sublimable cationic iridium(III) complexes with large steric hindrance for high-performance organic light-emitting diodes

*Ruihuan Liu[1], Dongxin Ma[1], Chen Zhang[1], Lian Duan[1,2]**

[1]Key Lab of Organic Optoelectronics & Molecular Engineering of Ministry of Education, Department of Chemistry, Tsinghua University, Beijing 100084, P. R. China;

[2]Center for Flexible Electronics Technology, Tsinghua University, Beijing 100084, P. R. China.

***Corresponding author E-mail:** duanl@mail.tsinghua.edu.cn

## Experimental Section

### General

$^{1}$H-NMR and $^{19}$F-NMR spectra were recorded on a JOEL JNM-ECA600 NMR spectrometer. ESI mass spectrometry was performed with Thermo Electron Corporation Finnigan LTQ. Absorption and photoluminescence (PL) spectra were characterized with an ultraviolet-visible spectrophotometer (Agilent 8453) and a fluorospectrophotometer (HITACHI, F-7000), respectively. Photoluminescence quantum yields (PLQYs) in degassed anhydrous acetonitrile solutions and neat film were measured at the excitation wavelength of 400 nm (Hamamutsu Photonics K. K., C9920-03). The excited state lifetimes were measured by a lifetime and steady state spectrometer (Edinburgh Instruments, FLS 980) with time-correlated single-photon counting technique at the peak emitting wavelength. Cyclic voltammetry was proved in oxygen-free anhydrous solutions on a Princeton Applied Research potentiostat/ galvanostat Model 283 voltammetric analyzer at a scan rate of 100 mV/s with a platinum plate as the working electrode, a silver wire as the pseudo-reference electrode and a platinum wire as the counter electrode. Oxidation potentials were measured in *N*,*N*-dimethyl formamide with tetrabutylammonium perchlorate (40 mg mL$^{-1}$) as the supporting electrolyte, while reduction potentials were performed in acetonitrile with tetrabutylammonium hexafluorophosphate (35 mg mL$^{-1}$) as the supporting electrolyte. Ferrocene served as the internal standard. Thermal stability was measured by a thermogravimetric analyzer (TA Instruments Q5000) with a heating rate of 10$^{o}$C min$^{-1}$ under nitrogen flows.

### Device fabrication and evaluation

OLEDs were grown on cleaned, ultraviolet-ozone-treated and indium-tin-oxide-coated glass substrates, with a sheet resistance of about 20 Ω per sq. Each functional layer was fabricated thereon successively by vacuum evaporation deposition under a low pressure below 5×10$^{-4}$ Pa. Each device shows an active area of 3.0×3.0 mm$^{2}$. Current density-luminance-voltage (J-L-V) characteristics were collected with Keithley 4200 semiconductor system, while electroluminescence (EL) spectra were recorded by a Photo Research PR705 spectrophotometer. Device measurements were carried out at room temperature in the ambient air without further encapsulations.

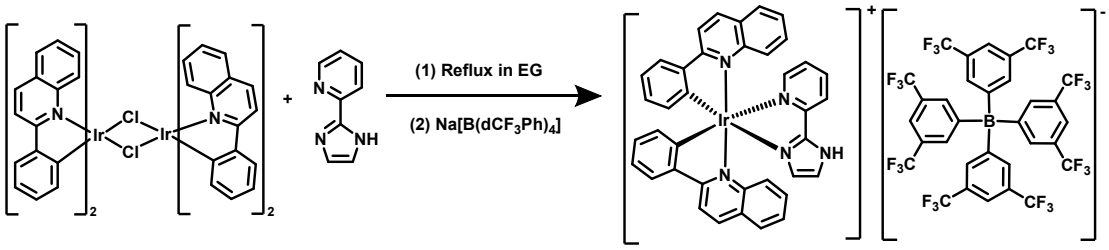


**Scheme S1** Synthetic routes of complexes **1**.

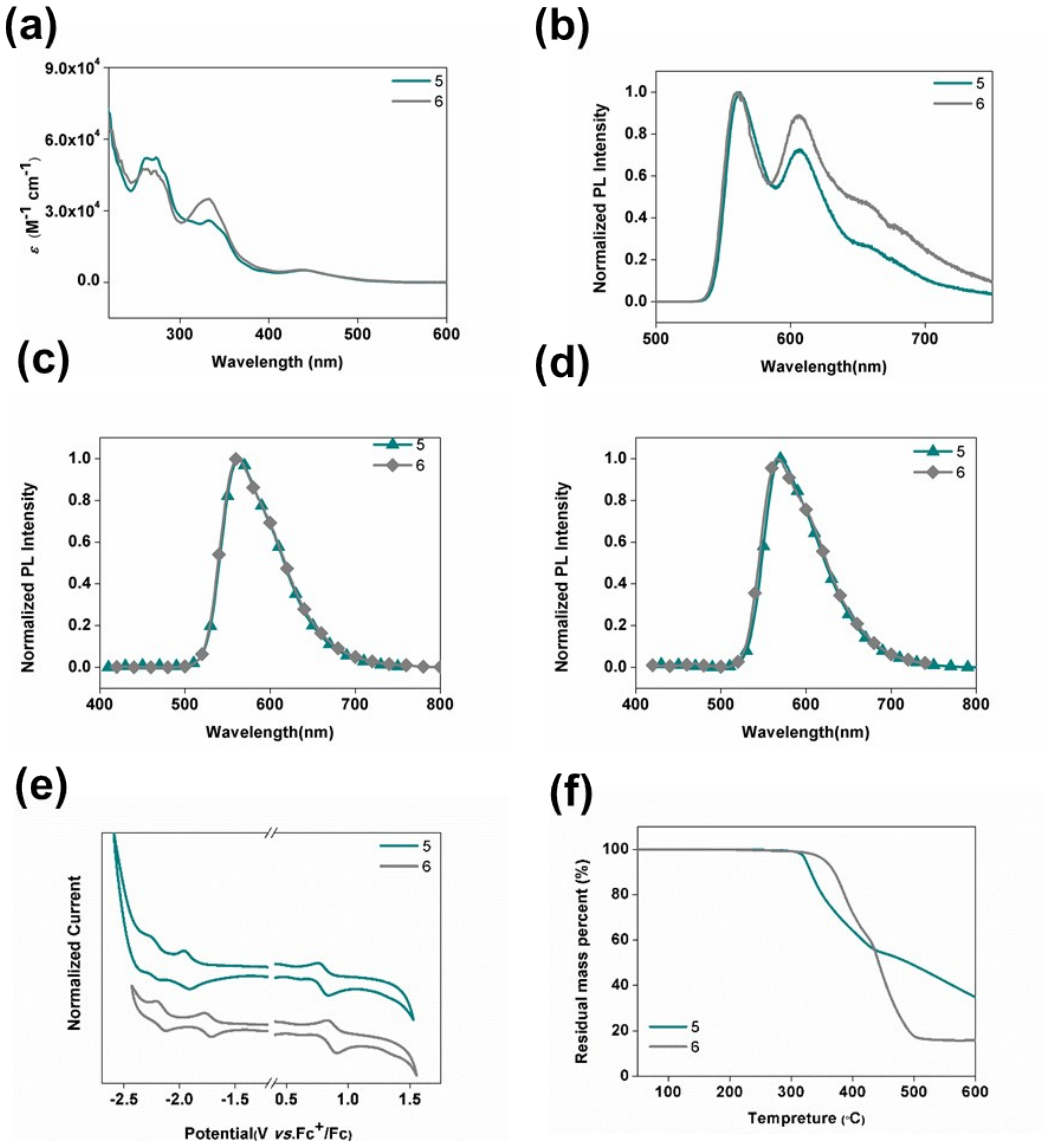


Fig. S1 (a) Absorption spectra, (b) PL spectra in oxygen-free acetonitrile solutions, (c) PL spectra in spin-coated neat films, and (d) PL spectra at 77 K. (e) Cyclic voltammogram, and (f) TGA under nitrogen-flow conditions of complexes **5** and **6**.

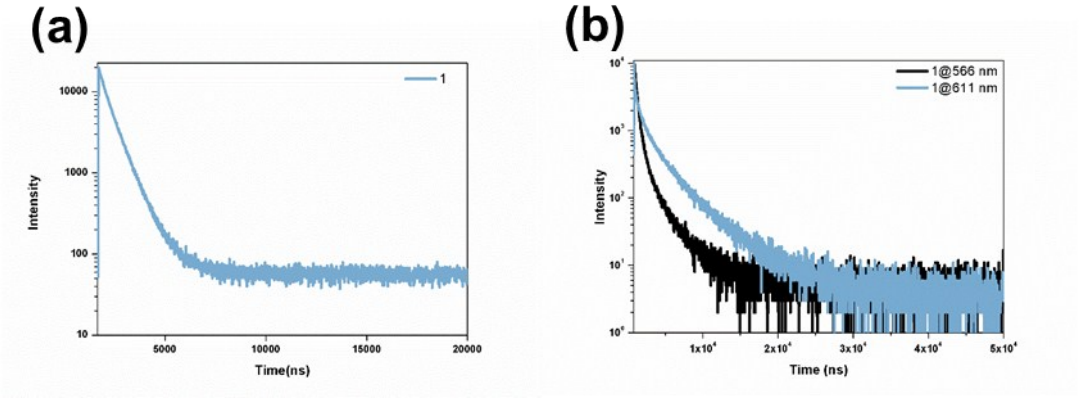


Fig. S2 Excited state lifetimes of complex **1** (a) in neat films at room temperature and (b) in acetonitrile glass at 77 K.

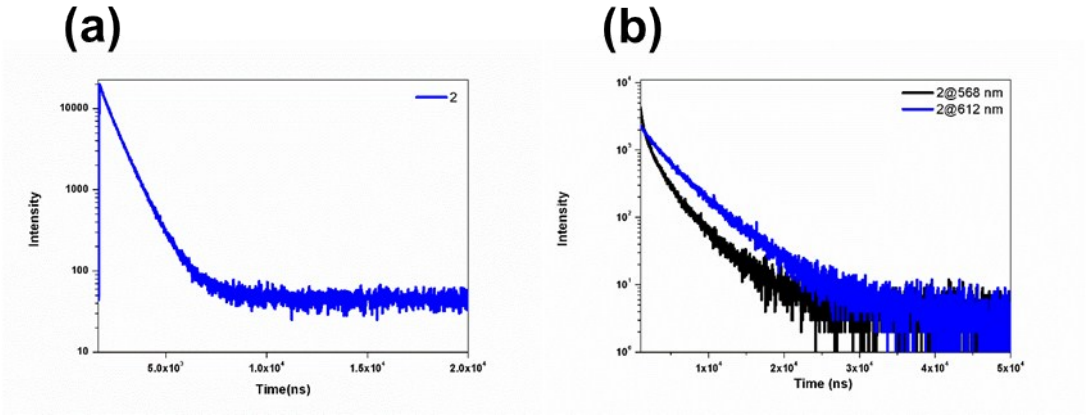


Fig. S3 Excited state lifetimes of complex **2** (a) in neat films at room temperature and (b) in acetonitrile glass at 77 K.

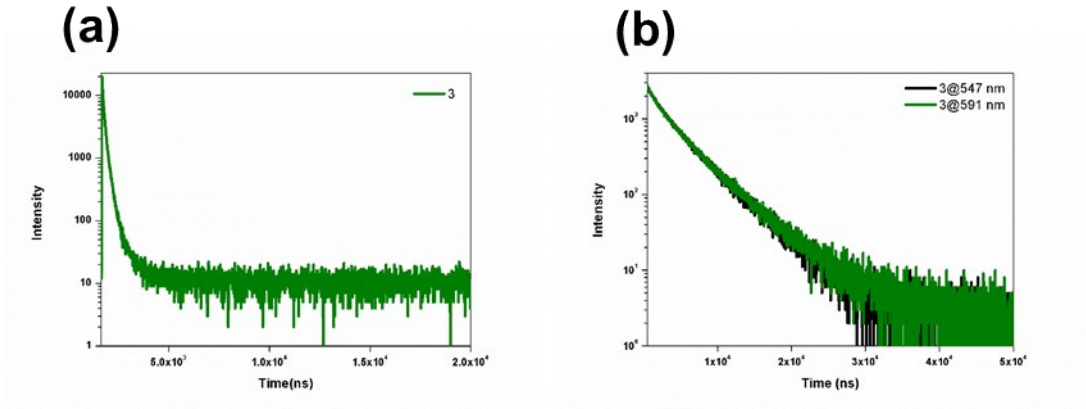


Fig. S4 Excited state lifetimes of complex **3** (a) in neat films at room temperature and (b) in acetonitrile glass at 77 K.

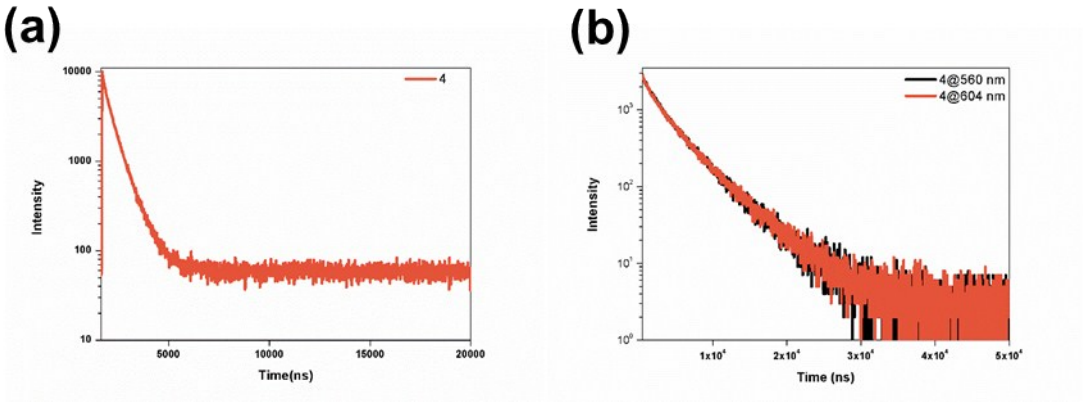


Fig. S5 Excited state lifetimes of complex **4** (a) in neat films at room temperature and (b) in acetonitrile glass at 77 K.

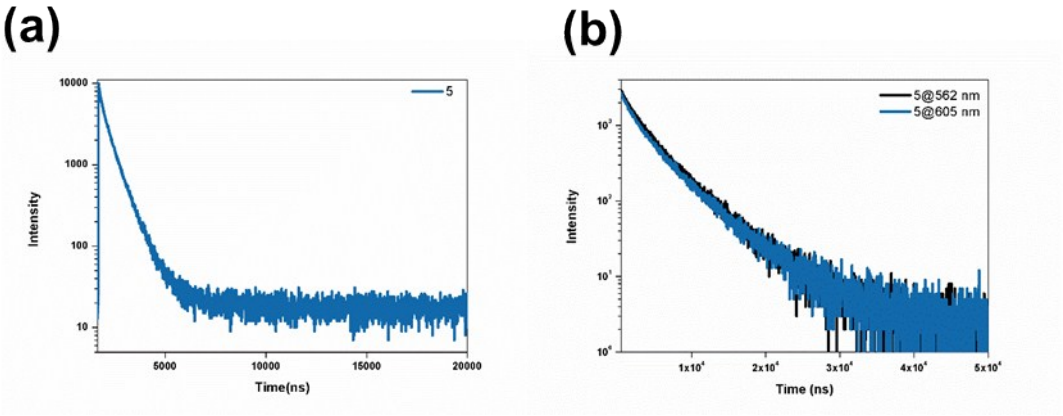


Fig. S6 Excited state lifetimes of complex **5** (a) in neat films at room temperature and (b) in acetonitrile glass at 77 K.

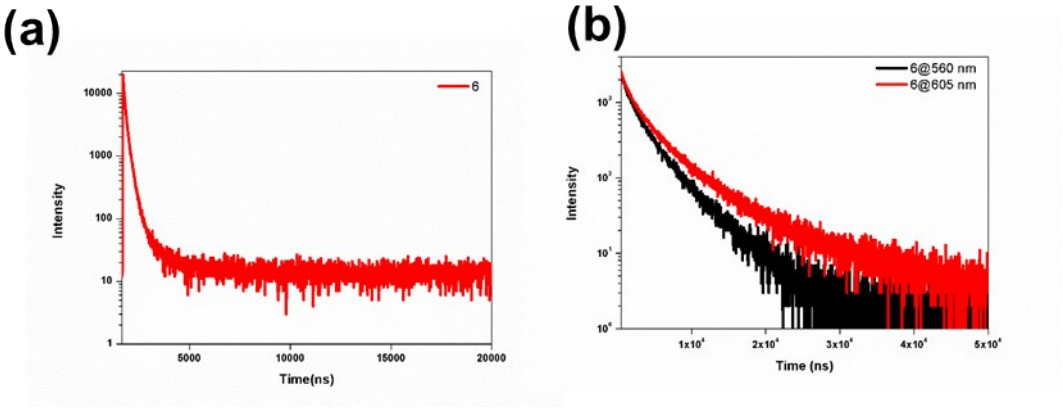


Fig. S7 Excited state lifetimes of complex **6** (a) in neat films at room temperature and (b) in acetonitrile glass at 77 K.

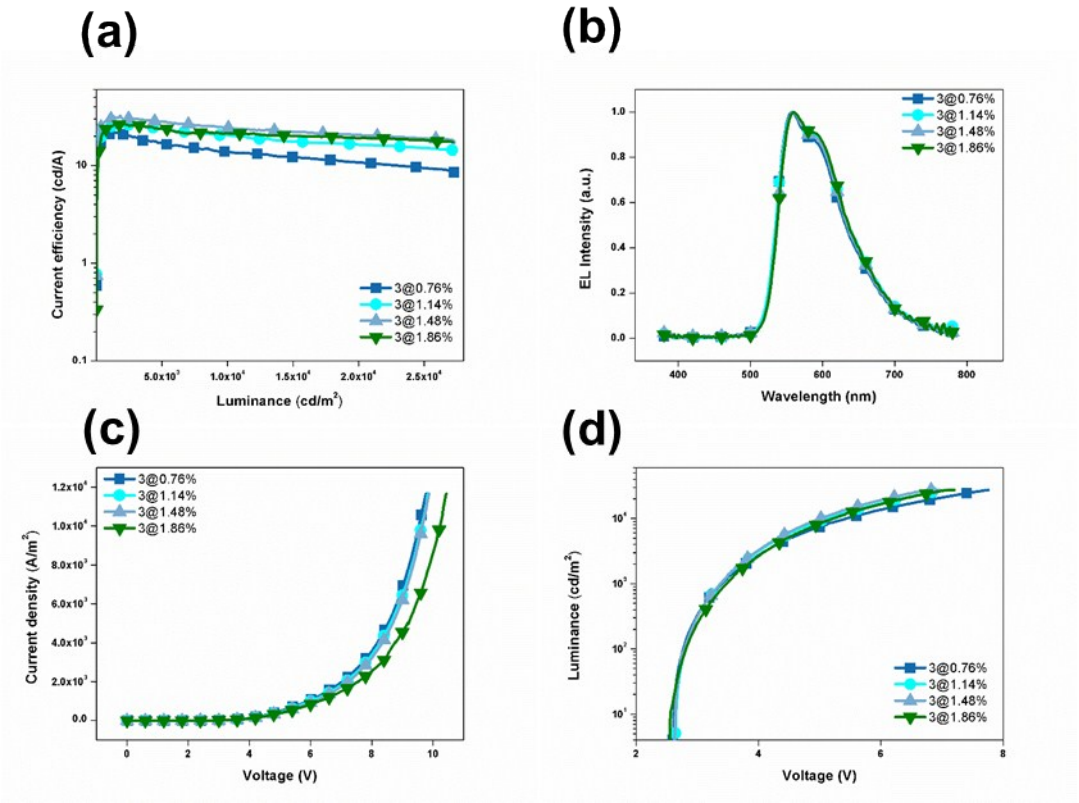


Fig. S8 Characteristics of the OLEDs based on complex **3** in the structure of ITO/ HATCN (5 nm)/ NPB (40 nm)/ TCTA (10 nm)/ DIC-TRZ: x% complex **3** (12 nm)/ BPBiPA (50 nm)/ LiF (1 nm)/ Al (150 nm) at varying dopant concentrations. (a) Current efficiency-luminance curves, (b) EL spectra and (c) Current density-voltage, (d) Luminance-voltage.

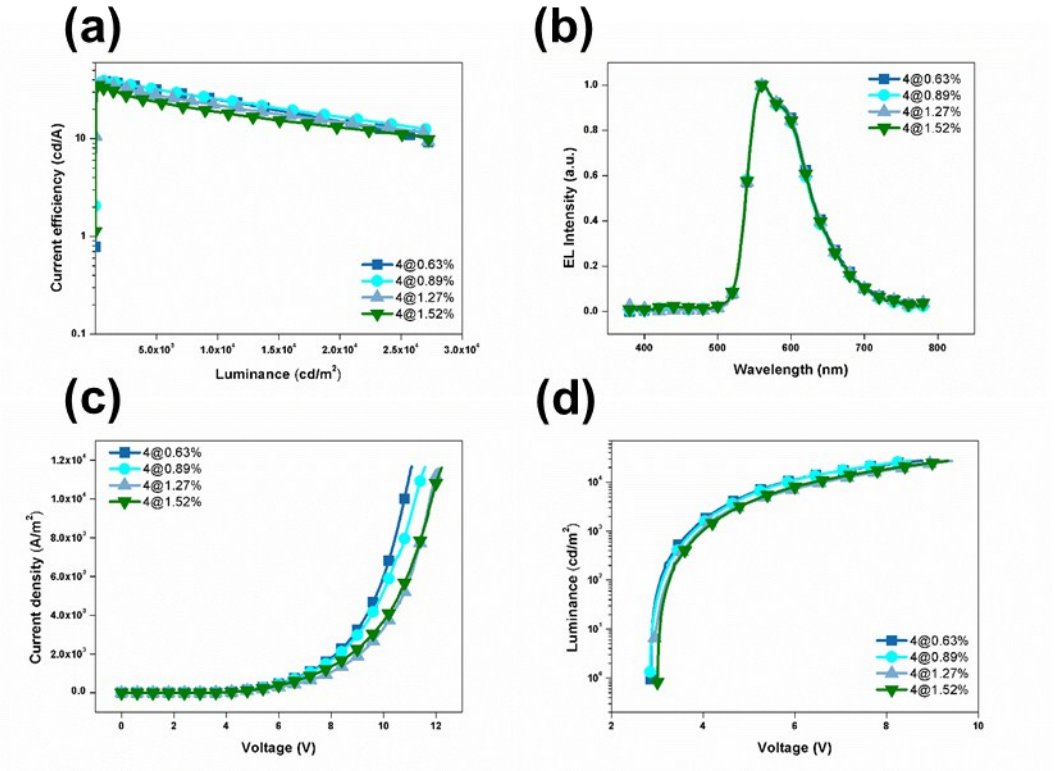

Fig. S9 Characteristics of the OLEDs based on complex **4** in the structure of ITO/ HATCN (5 nm)/ NPB (40 nm)/ TCTA (10 nm)/ DIC-TRZ: x% complex **4** (12 nm)/ BPBiPA (50 nm)/ LiF (1 nm)/ Al (150 nm) at varying dopant concentrations. (a) Current efficiency-luminance curves, (b) EL spectra and (c) Current density-voltage, (d) Luminance-voltage.

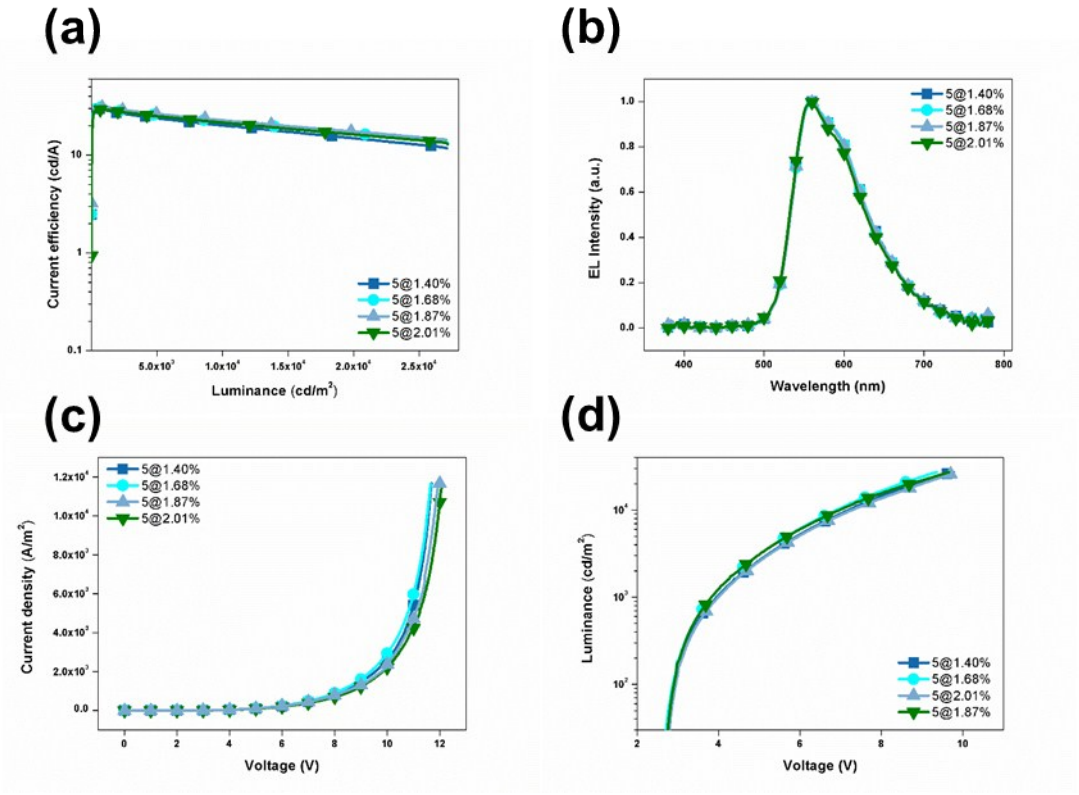


Fig. S10 Characteristics of the OLEDs based on complex **5** in the structure of ITO/ HATCN (5 nm)/ NPB (40 nm)/ TCTA (10 nm)/ DIC-TRZ: x% complex **5** (12 nm)/ BPBiPA (50 nm)/ LiF (1 nm)/ Al (150 nm) at varying dopant concentrations. (a) Current efficiency-luminance curves, (b) EL spectra and (c) Current density-voltage, (d) Luminance-voltage.

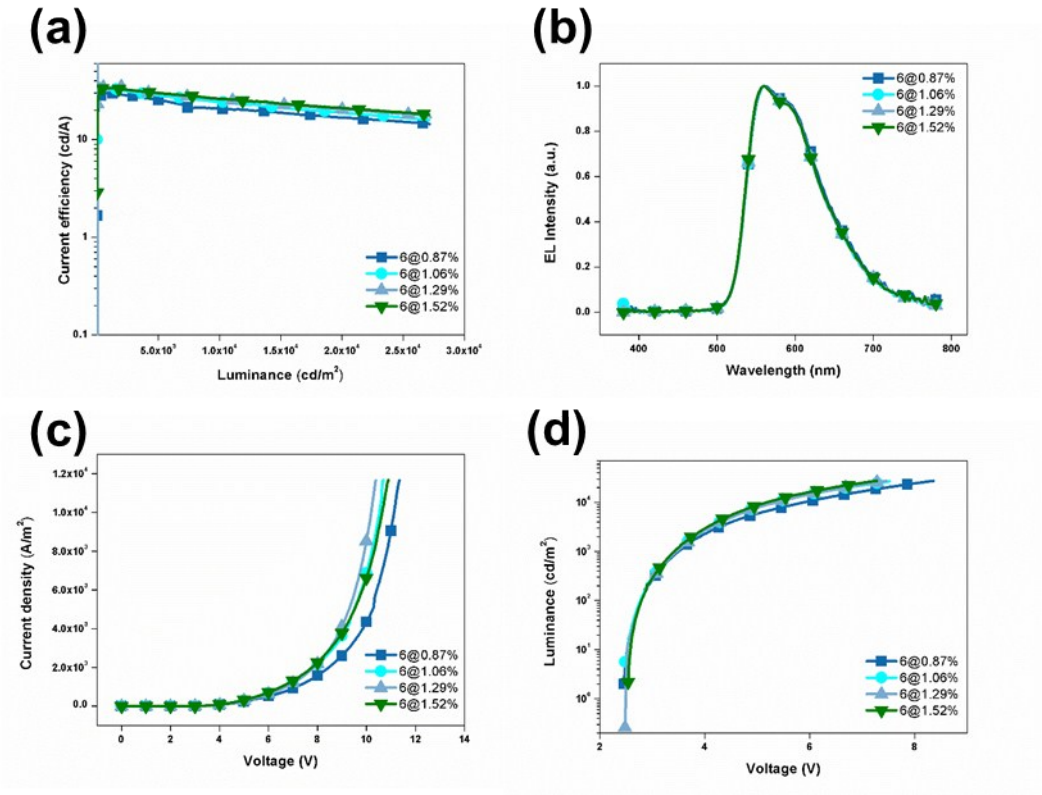


Fig. S11 Characteristics of the OLEDs based on complex **6** in the structure of ITO/ HATCN (5 nm)/ NPB (40 nm)/ TCTA (10 nm)/ DIC-TRZ: x% complex **6** (12 nm)/ BPBiPA (50 nm)/ LiF (1 nm)/ Al (150 nm) at varying dopant concentrations. (a) Current efficiency-luminance curves, (b) EL spectra and (c) Current density-voltage, (d) Luminance-voltage.

**Table S1** Device characteristics of yellow-emitting OLEDs based on complexes **1-6**.

| | Ratio [%] | $V_{on}$[a] [V] | Max CE[b] [cd $A^{-1}$] | CE[b] at $10^3$ cd $m^{-2}$ [cd $A^{-1}$] | CE[b] at $10^4$ cd $m^{-2}$ [cd $A^{-1}$] | Max EQE[c] [%] | Max PE[d] [lm $W^{-1}$] | Max $L$[e] [cd $m^{-2}$] | $\lambda_{EL}$[f] [nm] | CIE[g] ($x$, $y$) |
|---|---|---|---|---|---|---|---|---|---|---|
| 1 | 1.5 | 2.5 | 8.5 | 7.0 | 1.8 | 3.0 | 7.1 | $13.0\times10^3$ | 560, 592(*sh*) | (0.48,0.51) |
| 2 | 1.3 | 2.5 | 8.5 | 8.2 | 3.6 | 3.1 | 6.5 | $16.3\times10^3$ | 560, 592 (*sh*) | (0.49,0.50) |
| 3 | 0.8 | 2.3 | 23.0 | 21.1 | 13.8 | 8.3 | 20.7 | $>27.3\times10^3$ | 558, 591 (*sh*) | (0.49, 0.50) |
| | 1.1 | 2.2 | 27.5 | 24.6 | 20.3 | 10.1 | 24.3 | $>27.3\times10^3$ | 560, 591 (*sh*) | (0.49, 0.50) |
| | 1.5 | 2.2 | 32.4 | 30.0 | 24.5 | 11.9 | 28.3 | $>27.3\times10^3$ | 558, 591 (*sh*) | (0.49, 0.50) |
| | 1.9 | 2.2 | 27.4 | 25.0 | 21.3 | 10.2 | 23.5 | $>27.3\times10^3$ | 560, 593 (*sh*) | (0.50, 0.49) |
| 4 | 0.6 | 2.4 | 39.8 | 38.6 | 25.2 | 11.2 | 38.6 | $>27.3\times10^3$ | 560, 592 (*sh*) | (0.50, 0.49) |
| | 0.9 | 2.4 | 41.8 | 39.0 | 25.4 | 14.7 | 40.3 | $>27.3\times10^3$ | 560, 592 (*sh*) | (0.49, 0.49) |
| | 1.2 | 2.4 | 36.5 | 35.6 | 22.0 | 13.9 | 36.9 | $>27.3\times10^3$ | 560, 592 (*sh*) | (0.49, 0.50) |
| | 1.5 | 2.5 | 37.1 | 31.9 | 18.8 | 13.3 | 34.4 | $>27.3\times10^3$ | 560, 592 (*sh*) | (0.50, 0.49) |
| 5 | 1.4 | 2.4 | 32.5 | 29.0 | 20.1 | 11.4 | 33.8 | $>27.0\times10^3$ | 558, 591 (*sh*) | (0.48,0.51) |
| | 1.7 | 2.4 | 32.9 | 30.5 | 21.9 | 12.0 | 34.7 | $>27.0\times10^3$ | 558, 591 (*sh*) | (0.48,0.51) |
| | 1.9 | 2.4 | 31.2 | 30.8 | 22.7 | 10.9 | 32.3 | $>27.0\times10^3$ | 558, 591 (*sh*) | (0.48,0.51) |
| | 2.0 | 2.4 | 29.4 | 29.1 | 21.5 | 10.2 | 29.5 | $>27.0\times10^3$ | 558, 591 (*sh*) | (0.48,0.51) |
| 6 | 0.9 | 2.1 | 30.8 | 29.9 | 20.6 | 11.7 | 31.6 | $>27.3\times10^3$ | 560, 596 (*sh*) | (0.50, 0.49) |
| | 1.1 | 2.2 | 37.8 | 33.4 | 24.3 | 14.1 | 40.9 | $>27.3\times10^3$ | 560, 596 (*sh*) | (0.50, 0.49) |
| | 1.3 | 2.2 | 38.1 | 33.9 | 25.8 | 14.3 | 41.0 | $>27.3\times10^3$ | 560, 596 (*sh*) | (0.50, 0.49) |
| | 1.5 | 2.2 | 36.0 | 33.7 | 26.1 | 13.5 | 39.0 | $>27.3\times10^3$ | 560, 596 (*sh*) | (0.50, 0.50) |

[a] $V_{on}$, turn-on voltage. [b] CE, current efficiency. [c] EQE, external quantum efficiency. [d] PE, power efficiency. [e] $L$, luminance. [f] $\lambda_{EL}$, EL wavelength, *sh* denotes the shoulder peak. [g] CIE, Commission Internationale de I'Elairage.